AIMS Mathematics, 10(8): 18887–18912.
DOI: 10.3934/math.2025844
Received: 04 July 2025
Revised: 03 August 2025
Accepted: 12 August 2025
Published: 20 August 2025

https://www.aimspress.com/journal/Math

Research article

Load frequency control with an event-triggered mechanism for nonlinear power systems based on the improved grey wolf optimization algorithm

Yan Chen[1], **Xingyue Liu**[1,*], **Fengying Zeng**[2], **Kaibo Shi**[1] **and Fanglu Yang**[2]

[1] School of Electronic Information and Electrical Engineering, Chengdu University, Chengdu 610106, Sichuan, China

[2] AECC Sichuan Gas Turbine Research Institute, Mianyang 621000, Sichuan, China

* **Correspondence:** Email: liuxingyue0828@163.com.

Abstract: This study focused on the load frequency control problem of power systems by integrating the event-triggered mechanism (ETM) and the improved grey wolf optimization (IGWO) algorithm. First, a nonlinear power system (NPS) model incorporating an energy storage system (ESS) and renewable energy sources (RESs) was constructed. The model considers the nonlinear characteristics of governors and turbines, and the takagi-sugeno (T-S) fuzzy theory is introduced to handle the nonlinear terms in the model. Subsequently, during the sampling process, an ETM is introduced, and the improved grey wolf algorithm is used to find the optimal event-triggered parameters to reduce unnecessary information transmission. Second, based on the Lyapunov functional, the stability criterion of the system under disturbance conditions was derived, a controller was designed, and the control gain was determined by solving linear matrix inequalities (LMIs). Finally, the performance differences between the traditional ETM and the ETM combined with IGWO were compared. The results show that the optimization method can further reduce the bandwidth resource consumption while ensuring system stability and control effectiveness.

Keywords: nonlinear power system; T-S fuzzy theory; load frequency control; event-triggered mechanism; improved grey wolf optimization algorithm
Mathematics Subject Classification: 93-XX

1. Introduction

In the context of rapid global economic development and continuous social progress, the scale of power systems has expanded exponentially, accompanied by a corresponding increase in operational complexity. Concurrently, driven by the "dual carbon" goals, the global energy structure is accelerating its transition toward low-carbon alternatives. Traditional energy generation models are grappling with

challenges such as fluctuating raw material prices and escalating environmental governance costs, leading to rising generation costs. Against this backdrop, RESs, exemplified by solar and wind power, are seeing a steady rise in their penetration within power systems due to their zero-carbon emissions and sustainable nature [1]. However, the stochastic and intermittent characteristics of RESs pose significant challenges to the stability of power systems. ESSs can dynamically regulate these issues through charge and discharge operations. Studies indicate that ESSs, with their rapid response capabilities and high ramping rates [2], can effectively mitigate frequency deviations and tie-line power fluctuations caused by RES integration. Consequently, constructing dynamic models of power systems that incorporate RESs and ESSs, and conducting in-depth research on system stability analysis and control strategies, have become pivotal research directions in the field of power system control.

In power systems, frequency is a critical electrical parameter [3, 4]. Frequency fluctuations often arise from imbalances between generation and load demands [5]. Load frequency control (LFC) systems maintain frequency and inter-area power exchange at set values by adjusting generator outputs to meet varying load demands [6–8], ensuring power quality. Reference [9] modeled LFC as a linear system and investigated model predictive control strategies to address wind power uncertainty. Reference [10] analyzed LFC in deregulated power markets under denial-of-service attacks using linearized models. However, with increasing RES integration, the volatility of power generation has grown significantly, rendering traditional linear LFC models inadequate for capturing system dynamics [3]. Consequently, recent years have witnessed a surge in research on control methods for nonlinear LFC models [11–13].

The nonlinear characteristics of power systems increase the difficulty in analyzing system stability and designing load frequency control (LFC) strategies. Currently, various control methods have been proposed by the academic and engineering communities for nonlinear systems [14–17]. For example, a distributed-decentralized control framework was developed in [18] for nonlinear power systems to replace the traditional hierarchical centralized control mode, which effectively solves the problems of poor flexibility and excessive communication burden in large-scale grid interconnections. In [19], nonlinear factors in the dynamic processes of steam turbines and governors were considered, a nonlinear LFC model was constructed, and a distributed output feedback control strategy suitable for nonlinear power systems was designed. In addition, T-S fuzzy control technology has become an important means to study nonlinear systems due to its advantage in integrating fuzzy logic with mature linear control theories [20, 21], and a series of valuable research results have been achieved through this technology in numerous studies [22, 23]. Based on the analysis and summary of existing studies, a unified T-S fuzzy LFC model will be constructed in this paper, which is the first research motivation of this paper.

With the digitalization of industrial production, continuous-time devices are being replaced by digital counterparts. Sampled-data methods, which achieve control objectives with limited information transmission, have become essential for optimizing communication resources and are widely used in various control processes. Reference [21] designed a sampled-data adaptive fuzzy output feedback controller for non-strict-feedback large-scale systems, overcoming traditional data constraints. Reference [22] proposed a new method for exponential stability criteria of asynchronous sampled linear systems. Meanwhile, event-triggered communication mechanisms significantly reduce network resource usage. Reference [23] integrated an improved ETM with adaptive dynamic programming for LFC in power systems. Reference [3] proposed a T-S fuzzy model-based ETM

for power system LFC. Event-triggered parameters play a crucial role in ETM performance, but conventional dynamic triggering algorithms have optimization limitations. Therefore, intelligent optimization algorithms should be considered for ETMs. Common algorithms include particle swarm optimization (PSO), firefly algorithms, and hybrid firefly algorithms. Compared to other optimization techniques, the grey wolf optimizer (GWO) algorithm offers advantages such as low computational complexity, high precision, and convergence without initial condition sensitivity [24]. Moreover, it excels at avoiding local optima and is widely used in optimization problems [25]. In this work, an IGWO algorithm is introduced to dynamically optimize ETM threshold parameters, leveraging the intelligent hunting behavior of wolf packs to achieve global parameter optimization. This constitutes the second motivation of this research.

Time delays are another critical factor affecting power system stability. Existing research on time-delay stability in power systems, despite employing various Lyapunov-Krasovskii functional (LKF) methods and inequality optimization techniques, still faces limitations. Methods such as augmented LKF [26] and multiple-integral LKF [27] often struggle with complex time-varying delays and strong nonlinearities due to their fixed functional forms, leading to conservative stability criteria. Integral estimation methods based on Jensen's inequality [28] and Wirtinger's inequality [29] may not tightly characterize time-delay boundaries in high-order systems or those with highly fluctuating parameters, increasing computational complexity and reducing engineering practicality. Therefore, this paper introduces a novel LKF by incorporating slack matrices and delay product terms, enhancing adaptability to time-varying delays and nonlinear dynamics. Combined with specific lemmas, this approach reduces criterion conservatism and simplifies calculations, enabling more accurate stability analysis of the T-S fuzzy model for the nonlinear LFC power system in this study. This is the third motivation of this research.

Building on the above motivations, this study innovatively proposes an ETM based on an IGWO algorithm for T-S nonlinear LFC system models. The T-S control rules are designed in conjunction with this mechanism, and the novel LKF is employed to analyze system stability, verifying the superiority and effectiveness of the proposed method. The main contributions are as follows:

(1) An NPS model incorporating ESS, RES, governor deadband, and turbine valve constraints is established, and T-S fuzzy theory is used to handle nonlinear terms.

(2) A dynamic ETM is proposed and optimized using an IGWO algorithm to minimize bandwidth resource consumption while ensuring stability.

(3) Based on Lyapunov stability theory, stability criteria compatible with time-varying delays and nonlinearities are derived. A novel LKF is constructed by introducing slack matrices and delay product terms, reducing criterion conservatism and computational complexity through relevant lemmas.

The structure of this paper is presented as follows: Section 2 models the NPS, applies T-S fuzzy theory to handle nonlinearities, and integrates the designed ETM. Section 3 details stability analysis and controller synthesis methods, as well as the optimization of the ETM using the IGWO algorithm. Section 4 validates the effectiveness of the proposed scheme through comparative simulations.

Notation: R^n denotes the n-dimensional Euclidean space; the transpose and inverse of matrix P are denoted as P^T and P^{-1}, respectively; $P > 0$ represents a positive definite matrix; $col\{x_1, ..., x_n\}$ denotes the vertical stacking of vectors; $Sym(P) = P + P^T$ is used to simplify symmetric matrix expressions; $\|\cdot\|$ is the Euclidean norm; $L_2[0, +\infty)$ refers to the space of square-integrable functions.

2. Problem formulation

In this section, an NPS model with ESS and RES is first established, the T-S fuzzy model is used to handle the nonlinear terms in the NPS model, and then an ETM is designed for it to reduce unnecessary information transmission. Finally, the required lemmas are given.

2.1. T-S fuzzy model of the NPS

In many published studies [30–32], the LFC model of a power system is usually established as the linearized equation shown below:

$$\begin{aligned}
\Delta\dot{f}(t) &= \frac{-D\Delta f(t) + \Delta p_t(t) - \Delta p_d(t)}{M}, \\
\Delta\dot{p}_t(t) &= \frac{-\Delta p_t(t) + \Delta p_g(t)}{T_t}, \\
\Delta\dot{p}_g(t) &= \frac{-\Delta f(t) - T_g\Delta p_g(t) + T_g\Delta p_c(t)}{T_g R},
\end{aligned} \tag{2.1}$$

where $\Delta f(t)$, $\Delta p_t(t)$, $\Delta p_g(t)$, $\Delta p_d(t)$, and $\Delta p_c(t)$ represent the frequency deviation, generator mechanical power deviation, turbine valve position deviation, load deviation and load reference setpoint deviation, respectively. Other parameters are listed in Table 1.

Table 1. Practical meaning of parameters.

M	Equivalent inertia constant
D	Damping coefficient
T_t	Turbine time constant
T_g	Governor time constant
R	Governor droop coefficient
T_s	ESS time constant
K_s	ESS unit regulation coefficient
ρ_s	ESS power deviation coefficient
K_f	Frequency deviation coefficient

It is usually assumed that the load deviation $\Delta p_d(t)$ is a bounded function, satisfying $\|\Delta p_d(t)\| \leq \bar{p}_d$, where $\bar{p}_d$ is a positive constant [33]. However, when the system is faced with large load changes, due to the physical limitations of the governor valve position [15,18], the linearized LFC model (2.1) may not accurately describe the dynamic characteristics of the system. Specifically, the mechanical structure of the turbine determines that its steam flow injection will be dynamically adjusted with the load reference setpoint deviation $\Delta p_c(t)$, but the turbine valve position deviation $\Delta p_g(t)$ has clear physical limits: its maximum opening position is $\Delta p_{g_{\max}}$ and the minimum closing position is $\Delta p_{g_{\min}}$. When $\Delta p_g(t)$ exceeds the interval $[\Delta p_{g_{\min}}, \Delta p_{g_{\max}}]$, the truncation effect of the valve will be reflected by the nonlinear function $\xi(\cdot)$. In general, the turbine valve position deviation $\Delta p_g(t)$ can be expressed by the nonlinear function $\xi(\Delta p_g(t))$ as follows:

$$\xi(\Delta p_g(t)) = \begin{cases} k \cdot \Delta p_g(t), & \Delta p_g(t) \in [\Delta p_{g,\min}, \Delta p_{g,\max}], \\ \xi_{\max}, & \Delta p_g(t) > \Delta p_{g,\max}, \\ \xi_{\min}, & \Delta p_g(t) < \Delta p_{g,\min}, \end{cases} \tag{2.2}$$

where k is the linear gain, and $\xi_{\max}$ and $\xi_{\min}$ are the saturation values.

The block diagram of load frequency control for an NPS with an ESS is shown in Figure 1. Under the nonlinear characteristics of valve position limitations and the influence of the ESS on the power system, the participation ratios of the governor and ESS are set as α_1 and α_2 satisfying $\sum_{i=1}^{2} \alpha_i = 1$. The nonlinear load frequency control model is established as Eq (2.3).

$$\begin{aligned} \Delta\dot{f}(t) &= \frac{-D\Delta f(t) + \Delta p_t(t) + \Delta p_e(t) - \Delta p_d(t) + \Delta p_{\mathrm{RES}}(t)}{M}, \\ \Delta\dot{p}_t(t) &= \frac{-\Delta p_t(t) + \xi(\Delta p_g(t))}{T_t}, \\ \Delta\dot{p}_g(t) &= \frac{-\Delta f(t) - R\xi(\Delta p_g(t)) + R\alpha_1 \Delta p_c(t)}{T_g R}, \\ \Delta\dot{p}_e(t) &= \frac{-\Delta p_e(t) + \alpha_2 \kappa_e \Delta p_c(t) - \rho_e \kappa_e \Delta f(t)}{T_e}. \end{aligned} \tag{2.3}$$

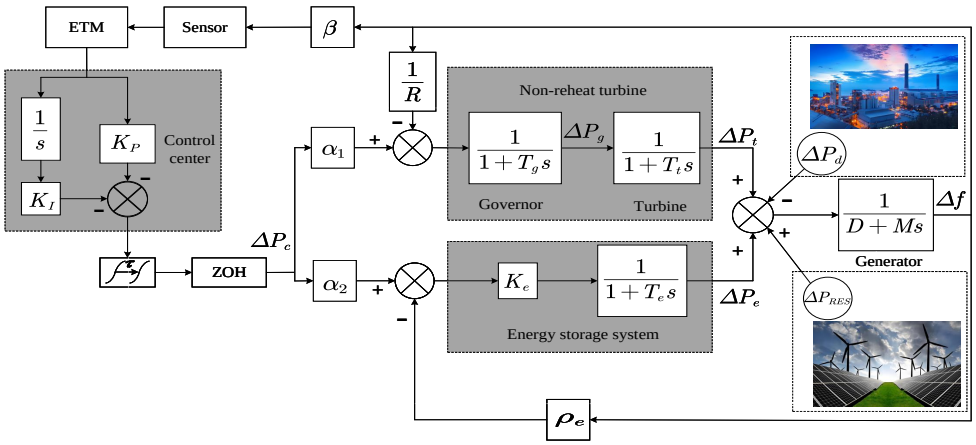

Figure 1. Framework of the LFC power system.

It is easy to obtain from Figure 1 that the proportional-integral (PI) controller can be written as $u(t) = -K_P \mathrm{ACE}(t) - K_I \int \mathrm{ACE}(t)dt$, where K_P is the proportional gain, K_I is the integral gain, and $\mathrm{ACE}(t)$ is the area control error. The controller output $u(t)$ can be defined as the load reference setpoint deviation $\Delta p_c(t)$, and the load deviation can be defined as the disturbance signal $w(t)$, i.e., $u(t) = \Delta p_c(t)$ and $w(t) = \Delta p_d(t)$. The area control error $\mathrm{ACE}(t)$ is proportional to the frequency deviation $\Delta f(t)$, with $\mathrm{ACE}(t) = \beta \Delta f(t)$, where β is the weight coefficient. Define the state vector $x(t)$ and output vector $y(t)$ to describe the system's dynamic state and controller design, respectively: $\bar{x}(t) = \mathrm{col}(\Delta f(t), \Delta p_t(t), \Delta p_g(t), \Delta p_e(t), \int \mathrm{ACE}(t))$, $\bar{y}(t) = \mathrm{col}(\mathrm{ACE}(t), \int \mathrm{ACE}(t))$. Considering the

above factors, the NPS model is established as follows, where $\phi(t)$ represents the initial condition:

$$\begin{cases} \dot{\bar{x}}(t) = A\bar{x}(t) + Bu(t) + Fw(t), \\ \bar{y}(t) = C\bar{x}(t), \\ \bar{x}(t) = \phi(t), \end{cases} \tag{2.4}$$

$$A = \begin{bmatrix} -\frac{D}{M} & \frac{1}{M} & 0 & \frac{1}{M} & 0 \\ 0 & -\frac{1}{T_t} & \frac{\xi(\Delta p_g(t))}{T_t \Delta p_g(t)} & 0 & 0 \\ -\frac{1}{T_g R} & 0 & -\frac{\xi(\Delta p_g(t))}{T_g \Delta p_g(t)} & 0 & 0 \\ -\frac{\rho_e K_e}{T_e} & 0 & 0 & -\frac{1}{T_e} & 0 \\ \beta & 0 & 0 & 0 & 0 \end{bmatrix}, \quad B = \begin{bmatrix} 0 \\ 0 \\ \frac{\alpha_1}{T_g} \\ \frac{\alpha_2 K_e}{T_e} \\ 0 \end{bmatrix}, \tag{2.5}$$

$$F = \begin{bmatrix} -\frac{1}{M} & 0 & 0 & 0 & 0 \end{bmatrix}^T, \quad C = \begin{bmatrix} \beta & 0 & 0 & 0 & 0 \\ 0 & 0 & 0 & 0 & 1 \end{bmatrix}.$$

To eliminate the nonlinear terms in the system model, the T-S fuzzy model is adopted to dynamically process the nonlinear function $\xi(\Delta p_g(t))$. The nonlinear LFC system can be described by the T-S fuzzy model as follows:

Plant rule i: If $\delta_1(\Delta p_g(t))$ belongs to $\mathcal{N}_{i_1}$, ... and $\delta_n(\Delta p_g(t))$ belongs to $\mathcal{N}_{i_n}$, ... and $\delta_{\bar{n}}(\Delta p_g(t))$ belongs to $\mathcal{N}_{i_{\bar{n}}}$, then:

$$\begin{cases} \dot{\bar{x}}(t) = A_i\bar{x}(t) + B_iu(t) + F_iw(t), \\ \bar{y}(t) = C_i\bar{x}(t), \\ \bar{x}(t) = \phi(t), \end{cases} \tag{2.6}$$

where $i = 1, 2, \ldots, m$, and m represents the number of fuzzy rules. $\delta_1(\Delta p_g(t)), \delta_2(\Delta p_g(t)), \ldots, \delta_{\bar{n}}(\Delta p_g(t))$ are premise variables. $\mathcal{N}_{i_1}, \mathcal{N}_{i_2}, \ldots, \mathcal{N}_{i_{\bar{n}}}$ are fuzzy sets. $B_i = B$, $F_i = F$, $C_i = C$, and the matrix A_i is expressed as:

$$A_i = \begin{bmatrix} -\frac{D}{M} & \frac{1}{M} & 0 & \frac{1}{M} & 0 \\ 0 & -\frac{1}{T_t} & \frac{\xi_i(\Delta p_g(t))}{T_t \Delta p_g(t)} & 0 & 0 \\ -\frac{1}{T_g R} & 0 & -\frac{\xi_i(\Delta p_g(t))}{T_g \Delta p_g(t)} & 0 & 0 \\ -\frac{\rho_e K_e}{T_e} & 0 & 0 & -\frac{1}{T_e} & 0 \\ \beta & 0 & 0 & 0 & 0 \end{bmatrix}. \tag{2.7}$$

Through defuzzification, system (2.6) can be transformed into:

$$\begin{cases} \dot{\bar{x}}(t) = \sum_{i=1}^{m} \nu_i(\delta(\Delta p_g(t))) \left(A_i\bar{x}(t) + B_iu(t) + F_iw(t)\right), \\ \bar{y}(t) = C_i\bar{x}(t), \\ \bar{x}(t) = \phi(t), \end{cases} \tag{2.8}$$

where $\sum_{i=1}^{m} \nu_i(\delta(\Delta p_g(t))) = 1, \nu_i(\delta_n(\Delta p_g(t))) = \frac{\prod_{n=1}^{\bar{n}} \mathcal{N}_{i_n}(\delta_n(\Delta p_g(t)))}{\sum_{i=1}^{m} \prod_{n=1}^{\bar{n}} \mathcal{N}_{i_n}(\delta_n(\Delta p_g(t)))}$, and $\mathcal{N}_{i_n}(\delta_n(\Delta p_g(t)))$ denotes the membership degree of $\delta_n(\Delta p_g(t))$ in the fuzzy set $\mathcal{N}_{i_n}$. To achieve stable control of system (2.8), a fuzzy PI control strategy is designed:

Plant rule j: If $\delta_1(\Delta p_g(t))$ belongs to $\mathcal{N}_{j_1}, \ldots,$ and $\delta_n(\Delta p_g(t))$ belongs to $\mathcal{N}_{j_q}, \ldots, \delta_{\bar{n}}(\Delta p_g(t))$ belongs to $\mathcal{N}_{j_{\bar{n}}}$, then:

$$u(t) = -K_{P_j}\mathrm{ACE}(t) - K_{I_j}\int \mathrm{ACE}(t)dt, \tag{2.9}$$

where K_{P_j} and K_{I_j} $(j = 1, 2, \ldots, m)$ are the proportional control gain and integral control gain, respectively. The expression of the defuzzified PI control strategy is:

$$u(t) = -\sum_{j=1}^{m} \nu_j(\delta(\Delta p_g(t)))K_{P_j}\mathrm{ACE}(t) - \sum_{j=1}^{m} \nu_j(\delta(\Delta p_g(t)))K_{I_j}\int \mathrm{ACE}(t)dt. \tag{2.10}$$

Substituting (2.10) into system (2.8) and letting $K_j = [K_{P_j}\ K_{I_j}]$, we obtain:

$$\begin{cases} \dot{\bar{x}}(t) = \sum\limits_{i=1}^{m}\sum\limits_{j=1}^{m} \nu_i(\delta(\Delta p_g(t)))\nu_j(\delta(\Delta p_g(t)))(A_i\bar{x}(t) - B_iK_jC_i\bar{x}(t) + F_iw(t)), \\ \bar{y}(t) = C_i\bar{x}(t), \\ \bar{x}(t) = \phi(t). \end{cases} \tag{2.11}$$

The unified fuzzy LFC model (2.11) for the power system has been established. Subsequently, the ETM will be incorporated into this model to achieve an integrated framework.

Remark 2.1. *The number of fuzzy rules m is related to the fuzzy subsets of input variables. Generally speaking, if there are m fuzzy subsets for a variable, then the TS fuzzy rules of the LFC system are m [34]. At the same time, different values of m also affect model accuracy and computational complexity: when m is small, the number of rules is small, the calculation process is simpler, and the demand for computing resources can be reduced. However, due to insufficient coverage of rules, the model may not accurately describe complex scenarios, thereby affecting the control effect. When m is large, the rules can more meticulously depict the changes of input variables, and the model accuracy tends to improve. However, this will significantly increase computational complexity, which may not only prolong the operation time but also cause overfitting risks due to problems such as rule redundancy. Therefore, in practical applications, it is necessary to weigh and select an appropriate m value in combination with specific scenarios.*

2.2. T-S fuzzy LFC model integrated with event-triggered fuzzy control

During the information interaction in the power system communication network, sensors sample data periodically and transmit it at fixed times, which occupies a large amount of bandwidth resources. Therefore, it is necessary to optimize the resource consumption of network bandwidth. In this study, an ETM is adopted to reduce unnecessary information transmission. Data is only transmitted when the system state changes drastically, thereby saving network communication resources.

Let h be the sampling interval of the sensor, mh represent the sampling moment, and $x(mh)$ denote the current sampling state. The sequence $\{t_kh\}$ characterizes the transmission moments of the sampling states, where $x(t_kh)$ represents the latest transmitted state. The interval h_k between adjacent transmission moments satisfies: $h \le h_k \triangleq t_{k+1}h - t_kh \le \bar{h}$. In general, the transmission moment sequence $\{t_kh\}$ of the ETM needs to satisfy the following condition [11]:

$$t_{k+1}h = \inf_{m\in\mathbb{N}}\left\{mh > t_kh \mid e^T(t)C^T\Omega Ce(t) \ge \varepsilon x^T(t_kh)C^T\Omega Cx(t_kh)\right\}, \tag{2.12}$$

where the matrix Ω is a positive definite unknown matrix , and the parameter ε takes a positive value with a range of $(0, 1)$. The defined $e(t)$ here is the error between the latest transmitted state and the current sampling state, i.e., $e(t) = x(t_k h) - x(mh)$. This mechanism decides whether to execute the transmission of the sampling signal by judging whether the above threshold condition is satisfied, that is, the signal transmission is triggered when the state error satisfies the preset matrix quadratic inequality. Due to the communication delay in the power system, when $t \in [t_k h + \tau_{t_k}, t_{k+1} h + \tau_{t_{k+1}}]$, it can be obtained that $ACE(t) = ACE(t_k h)$. Considering the ETM, the proportional-integral controller (PI controller) can be written as:

$$u(t) = -\sum_{j=1}^{m} \nu_j(\delta(\Delta p_g(t)))K_{P_j} ACE(t_k h) - \sum_{j=1}^{m} \nu_j(\delta(\Delta p_g(t)))K_{I_j} \int ACE(t_k h)dt. \tag{2.13}$$

At this time, the NPS can be transformed into the following form:

$$\begin{cases} \dot{\bar{x}}(t) = \sum_{i=1}^{m}\sum_{j=1}^{m} \nu_i(\delta(\Delta p_g(t)))\nu_j(\delta(\Delta p_g(t)))(A_i\bar{x}(t) - B_i K_j C_i \bar{x}(t_k h) + F_i w(t)), \\ \bar{y}(t) = C_i \bar{x}(t), \\ \bar{x}(t) = \phi(t). \end{cases} \tag{2.14}$$

Let $\tau(t) = t - mh$, where $t \in [mh, (m + 1)h)$, and obviously $\tau(t) \in [0, h)$. Combining the aforementioned error definition, the multi-area NPS under the communication network can be modeled as:

$$\begin{cases} \dot{\bar{x}}(t) = \sum_{i=1}^{m}\sum_{j=1}^{m} \nu_i(\delta(\Delta p_g(t)))\nu_j(\delta(\Delta p_g(t)))(A_i\bar{x}(t) - B_i K_j C_i \bar{x}(t - \tau(t)) - B_i K_j C_i e(t) + F_i w(t)), \\ \bar{y}(t) = C_i \bar{x}(t), \\ \bar{x}(t) = \phi(t),\ t \in [mh, (m + 1)h). \end{cases} \tag{2.15}$$

Remark 2.2. *In an ETM, the value of ε affects the triggering frequency and system performance. In terms of triggering frequency, the larger the ε, the stricter the triggering condition, the lower the triggering frequency , and the fewer the number of transmissions. The smaller the ε, the lower the triggering threshold, the higher the triggering frequency, and the greater the number of transmissions. In terms of system performance, an excessively large ε can reduce bandwidth occupancy but may affect system stability and control accuracy due to delayed transmission of key state information. An excessively small ε is beneficial to system stability but will cause waste of bandwidth resources due to frequent triggering, which violates the design intent of the ETM. Therefore, the optimal value of ε is found through global parameter optimization by IGWO, ensuring system stability while reducing triggering frequency and bandwidth resource consumption.*

Remark 2.3. *The event-triggered mechanism (2.12) is a periodic event-triggered mechanism. It periodically samples the system states at a fixed interval h via sensors. Information transmission is determined based on the triggering condition only at the sampling instants, instead of through continuous monitoring of the system states. This periodic characteristic has two notable advantages: First, it avoids resource consumption caused by continuous monitoring. Compared with continuous*

event-triggered mechanisms, the proposed mechanism makes judgments only at discrete sampling instants, which significantly reduces the monitoring burden of sensors. Second, it inherently avoids Zeno behavior. Zeno behavior refers to the phenomenon where event-triggered instants occur infinitely densely within a finite time, resulting in meaningless high-frequency transmissions in the system. In the proposed mechanism, the interval between adjacent sampling instants is strictly restricted to $h \leq h_k \leq \bar{h}$*. At most, the trigger instant coincides with the sampling instant, and the sampling interval* h *is a fixed positive value. This ensures that the interval between any two triggered instants is no less than* h*, preventing Zeno behavior.*

2.3. Basic lemmas

Lemma 2.1. *[35] For given matrices* Y*,* M *of appropriate dimensions and a matrix* Ψ*, if the inequality* $\Psi + Y\Delta(t)M + Y^T\Delta^T(t)M^T < 0$ *holds, and the unknown matrix* $\Delta(t)$ *satisfies* $\Delta^T(t)\Delta(t) \leq I$*, then for any positive scalar* ϑ*, the following inequality holds:* $\Psi + \vartheta Y\Delta(t)M + \vartheta M^T\Delta^T(t)Y^T < 0$*.*

Lemma 2.2. *[36] Let the function* $\varpi(\cdot) : [a, b] \to \mathbb{R}^n$ *be a differentiable function. For any matrices* G_i *(*$i = 1, 2, 3$*) and a positive definite matrix* $\Xi > 0$*, the following equality holds:*

$$-\int_a^b \dot{\varpi}^T(s)\Xi\dot{\varpi}(s)ds \leq (b-a)\zeta^T\left(G_1\Xi^{-1}G_1^T + \frac{1}{3}G_2\Xi^{-1}G_2^T + \frac{1}{5}G_3\Xi^{-1}G_3^T\right)\zeta + Sym\left\{\zeta^T\left(G_1\eta_1 + G_2\eta_2 + G_3\eta_3^{(i)}\right)\right\}, \quad (i = 1, 2),$$

where

$$\zeta_i = col\left\{\varpi(b), \varpi(a), \int_a^b \frac{\varpi(s)}{b-a}\,ds, \int_a^b\int_a^\rho \frac{\varpi(s)}{(b-a)^2}\,ds\,d\rho\right\},$$

$$\eta_1 = \varpi(b) - \varpi(a), \eta_2 = \varpi(b) + \varpi(a) - \frac{2}{b-a}\int_a^b \varpi(s)\,ds,$$

$$\eta_3^{(1)} = \varpi(b) - \varpi(a) - 6\int_a^b \frac{\varpi(s)}{b-a}\,ds + 6\int_a^b\int_a^\rho \frac{\varpi(s)}{(b-a)^2}\,ds\,d\rho,$$

$$\eta_3^{(2)} = \varpi(b) - \varpi(a) + 6\int_a^b \frac{\varpi(s)}{b-a}\,ds - 6\int_a^b\int_a^\rho \frac{\varpi(s)}{(b-a)^2}\,ds\,d\rho,$$

are vectors of appropriate dimensions.

3. Main results

In this section, a Lyapunov functional is first used to analyze the stability of the system under disturbance, and then a controller design method is proposed. The control gain can be obtained by solving its LMIs, and the IGWO algorithm is used to optimize the ETM to find the optimal event-triggered threshold.

3.1. Stability analysis and controller design

In the field of load frequency control for power systems, H_∞ control is widely used to enhance the robustness of the system. The core of H_∞ control lies in ensuring through optimal design that the

H_∞ norm of the closed-loop system is less than a preset positive number γ. This norm reflects the gain of the system from the disturbance input to the controlled output. When $\omega(t) = 0$, the NPS is asymptotically stable. When $\omega(t) \in L_2[0, \infty)$, there exists a positive scalar γ such that under zero initial conditions, $\|y(t)\| \leq \gamma\|\omega(t)\|_2$ is satisfied. By limiting this norm, H_∞ control can effectively suppress the influence of external disturbances and system uncertainties on system performance in the worst-case scenario [11].

The following matrices are defined to facilitate the stability analysis of the system:

$$\begin{aligned}
&\theta(t) = \mathrm{col}\begin{Bmatrix}\bar{x}(t), \dot{\bar{x}}(t), \bar{x}(t-\tau_M), \dot{\bar{x}}(t-\tau_M), u(t), \dot{u}(t), v(t), \dot{v}(t),\\ \delta(t), \dot{\delta}(t), \bar{x}(t_k h), w_1(t), w_2(t), \bar{x}(t-\tau(t)), w(t)\end{Bmatrix},\\
&\theta_1(t) = \mathrm{col}\{\overline{x}(t), \overline{x}(t-\tau_M), u(t), v(t)\}, \theta_2(s) = \overline{x}(s) - \overline{x}(t_k h),\\
&\theta_3(t) = \mathrm{col}\{\overline{x}(t), \overline{x}(t-\tau_M), \delta(t)\}, \theta_4(t) = \mathrm{col}\{\overline{x}(t), \dot{\overline{x}}(t)\},\\
&w_1(t) = \frac{1}{t - t_k h}\int_{t_k h}^{t} x(\rho)\, d\rho, w_2(t) = \frac{1}{t_{k+1}h - t}\int_{t}^{t_{k+1}h} x(\rho)\, d\rho.
\end{aligned} \tag{3.1}$$

Theorem 3.1. *For a given parameter τ_M, if there exist positive scalars α, β, σ, positive definite matrices P, Q, R_i $(i = 1, 2, 3)$, Ω, W, a matrix $X = col\{X_1, X_2\}$ of appropriate dimensions, and arbitrary matrices M_i $(i = 1, 2)$, N_i $(i = 1, 2)$ such that $\begin{bmatrix} R & S^T \\ * & R \end{bmatrix} > 0$, the system (2.15) is asymptotically stable and has H_∞ performance with index γ. When $\tau(t) = 0$ or τ_M, the following inequalities hold:*

$$\begin{bmatrix} \Psi|_{\tau(t)} + h_k\Gamma_4 & \Upsilon_1 & \Upsilon_3 \\ * & -\Xi_1 & 0 \\ * & * & -\Xi_3 \end{bmatrix} < 0, \tag{3.2}$$

$$\begin{bmatrix} \Psi|_{\tau(t)} + h_k\Gamma_3 & \Upsilon_2 & \Upsilon_3 \\ * & -\Xi_2 & 0 \\ * & * & -\Xi_3 \end{bmatrix} < 0, \tag{3.3}$$

where

$$
\begin{aligned}
&\Psi = \sum_{i=0}^{6} \Psi_i, \Psi_1 = \alpha \cdot Sym\{e_2^T W(e_1 - e_{11})\},\\
&\Psi_2 = Sym\{\Pi_1^T P \Pi_2\} + e_1^T Q e_1 - e_3^T Q e_3,\\
&\Psi_3 = \tau_M^2 e_2^T R_3 e_2 + \beta t_e Sym\{\Pi_3^T R_3 \Pi_3 + t_e \Pi_4^T R_3 \Pi_3\},\\
&\Psi_4 = Sym\{\Pi_9^T M_1 \Pi_5 + \Pi_9^T M_2 \Pi_6\} + Sym\{\Pi_{10}^T \mathcal{N}_1 \Pi_7 + \Pi_{10}^T \mathcal{N}_2 \Pi_8\},\\
&\Psi_5 = \Pi_{11}^T \begin{bmatrix} R & S^T \\ * & R \end{bmatrix} \Pi_{11}, \Psi_6 = Sym\{I_1 I_2\} + e_1^T \overline{C}^T \overline{C} e_1 - e_{15}^T \gamma^2 I e_{15},\\
&I_1 = e_1^T X_1 + e_2^T X_2, \quad I_2 = \overline{A} e_1 - e_2 + \overline{B} e_5 + \overline{F} e_7, \Upsilon_1 = \begin{bmatrix} \sqrt{h_k}\Pi_{10}^T \mathcal{N}_1 & \sqrt{h_k}\Pi_{10}^T \mathcal{N}_2 \end{bmatrix},\\
&\Upsilon_2 = \begin{bmatrix} \sqrt{h_k}\Pi_9^T M_1 & \sqrt{h_k}\Pi_9^T M_2 \end{bmatrix}, \Upsilon_3 = \begin{bmatrix} \sigma I_1 H & \Pi_{12}^T \begin{bmatrix} \overline{C}D & \overline{C}D \end{bmatrix}^T \end{bmatrix},\\
&\Gamma_1 = \Pi_9^T \sum_{j=1}^{2} \frac{1}{2j-1} M_j R_1^{-1} M_j^T \Pi_9, \Gamma_2 = \Pi_{10}^T \sum_{j=1}^{2} \frac{1}{2j-1} \mathcal{N}_j R_2^{-1} \mathcal{N}_j^T \Pi_{10},\\
&\Xi_1 = diag\{R_2, 3R_2\}, \Xi_2 = diag\{R_1, 3R_1\}, \Xi_3 = diag\{\sigma I, \sigma I\}, \Gamma_3 = e_2^T R_2 e_2,\\
&\Pi_1 = col\{e_2, e_4, e_6, e_8\}, \Pi_2 = col\{e_1, e_3, e_5, e_7\}, \Pi_3 = col\{e_1, e_3, e_9\}, \Gamma_4 = e_2^T R_1 e_2,\\
&\Pi_4 = col\{e_2, e_4, e_{10}\}, \Pi_5 = e_1 - e_{11}, \Pi_6 = e_1 + e_{11} - 2e_{12}, \Pi_7 = e_{14} - e_1,\\
&\Pi_8 = e_1 + e_{14} - 2e_{13}, \Pi_9 = col\{e_1, e_{11}, e_{12}\}, \Pi_{10} = col\{e_{14}, e_1, e_{13}\},\\
&\Pi_{11} = col\{e_1 - e_{14}, e_{14} - e_3\}, \Pi_{12} = col\{e_5, e_7\}, e_i = \begin{bmatrix} 0_{n\times(i-1)n} & I_n & 0_{n\times(10-i)n} \end{bmatrix}.
\end{aligned} \tag{3.4}
$$

Proof. We use the following LKF to analyze the stability of the system under disturbances:

$$
\begin{aligned}
&V(t) = \sum_{i=1}^{4} V_i(t), V_1(t) = \alpha \cdot \theta_2^T(t) W \theta_2(t),\\
&V_2(t) = \theta_1^T(t) P \theta_1(t) + \int_{t-\tau_M}^{t} \overline{x}^T(s) Q \overline{x}(s)\, ds,\\
&V_3(t) = (t_{k+1}h - t) \int_{t_k h}^{t} \dot{\overline{x}}^T(s) R_1 \dot{\overline{x}}(s)\, ds - (t - t_k h) \int_{t}^{t_{k+1}h} \dot{\overline{x}}^T(s) R_2 \dot{\overline{x}}(s)\, ds,\\
&V_4(t) = \tau_M \int_{-\tau_M}^{0} \int_{t+\rho}^{t} \dot{\overline{x}}^T(s) R_3 \dot{\overline{x}}(s)\, ds\, d\rho + \beta(t - t_k h)^2 \theta_3^T(t) R_3 \theta_3(t).
\end{aligned} \tag{3.5}
$$

Differentiating $V(t)$:

$$\begin{aligned}
\dot{V}(t) =& \sum_{i=1}^{4} \dot{V}_i(t), I = -\int_{t_k h}^{t} \dot{\bar{x}}^T(s) R_1 \dot{\bar{x}}(s) ds - \int_{t}^{t_{k+1}h} \dot{\bar{x}}^T(s) R_2 \dot{\bar{x}}(s) ds, \\
\dot{V}_1(t) =& \alpha \cdot (\dot{\theta}_2^T(t) W \theta_2(t) + \theta_2^T(t) W \dot{\theta}_2(t)) = \theta^T(t) \Psi_1 \theta(t), \\
\dot{V}_2(t) =& \dot{\theta}_1^T(t) P \theta_1(t) + \theta_1^T(t) P \dot{\theta}_1(t) + \bar{x}^T(t) Q \bar{x}(t) - \bar{x}^T(t-\tau_M) Q \bar{x}(t-\tau_M) = \theta^T(t) \Psi_2 \theta(t), \\
\dot{V}_3(t) =& (t_{k+1}h - t)\, \dot{\bar{x}}^T(t) R_1 \dot{\bar{x}}(t) + (t - t_k h)\, \dot{\bar{x}}^T(t) R_2 \dot{\bar{x}}(t) - \int_{t_k h}^{t} \dot{\bar{x}}^T(s) R_1 \dot{\bar{x}}(s) ds - \int_{t}^{t_{k+1}h} \dot{\bar{x}}^T(s) R_2 \dot{\bar{x}}(s) ds \\
=& (t_{k+1}h - t)\, \theta^T(t) \Gamma_4 \theta(t) + (t - t_k h)\, \theta^T(t) \Gamma_3 \theta(t) + I, \\
\dot{V}_4(t) =& \tau_M \int_{-\tau_M}^{0} \left[\dot{\bar{x}}^T(t) R_3 \dot{x}(t) - \dot{\bar{x}}^T(t+\rho) R_3 \dot{\bar{x}}(t+\rho) \right] d\rho + 2\beta(t - t_k h) \theta_3^T(t) R_3 \theta_3(t) \\
&+ \beta(t - t_k h)^2 Sym\{\dot{\delta}^T(t) R_3 \delta(t)\} = \tau_M^2 \dot{\bar{x}}^T(t) R_3 \dot{\bar{x}}(t) + \beta t_e Sym\{\theta_3^T(t) R_3 \theta_3(t) + t_e \dot{\theta}_3^T(t) R_3 \theta_3(t)\} \\
&- \tau_M \int_{t-\tau_M}^{t} \dot{\bar{x}}^T(s) R_3 \dot{\bar{x}}(s) ds = \theta^T(t) \Psi_3 \theta(t) - \tau_M \int_{t-\tau_M}^{t} \dot{\bar{x}}^T(s) R_3 \dot{\bar{x}}(s).
\end{aligned} \tag{3.6}$$

By Lemma 2.2, the integral term in $\dot{V}_3(t)$ can be transformed into the following form:

$$\begin{aligned}
& - \int_{t_k h}^{t} \dot{\bar{x}}^T(s) R_1 \dot{\bar{x}}(s) ds - \int_{t}^{t_{k+1}h} \dot{\bar{x}}^T(s) R_2 \dot{\bar{x}}(s) ds \\
\leq & \theta^T(t) \left((t - t_k h) \Pi_9^{\mathrm{T}} \sum_{j=1}^{2} \frac{1}{2j-1} M_j R_1^{-1} M_j^{\mathrm{T}} \Pi_9 + (t_{k+1}h - t) \Pi_{10}^{\mathrm{T}} \sum_{j=1}^{2} \frac{1}{2j-1} \mathcal{N}_j R_2^{-1} \mathcal{N}_j^{\mathrm{T}} \Pi_{10} \right) \theta(t) \\
& + \theta^T(t)\, \mathrm{Sym} \left\{ \Pi_9^{\mathrm{T}} M_1 \Pi_5 + \Pi_9^{\mathrm{T}} M_2 \Pi_6 \right\} \theta(t) + \theta^T(t)\, \mathrm{Sym} \left\{ \Pi_{10}^{\mathrm{T}} \mathcal{N}_1 \Pi_7 + \Pi_{10}^{\mathrm{T}} \mathcal{N}_2 \Pi_8 \right\} \theta(t) \\
= & \theta^T(t) \left(\Psi_4 + (t - t_k h) \Gamma_1 + (t_{k+1}h - t) \Gamma_2 \right) \theta(t).
\end{aligned} \tag{3.7}$$

Through the reciprocal convex method for time-varying delay systems in [37], the integral term in $\dot{V}_4(t)$ can be converted into the following form:

$$\begin{aligned}
-\tau_M \int_{t-\tau_M}^{t} \dot{\bar{x}}^T(s) R_3 \dot{\bar{x}}(s)\, ds \leq & - \begin{bmatrix} \bar{x}(t) - \bar{x}(t - \tau(t)) \\ \bar{x}(t - \tau(t)) - \bar{x}(t - \tau_M) \end{bmatrix}^T \begin{bmatrix} R & S^T \\ * & R \end{bmatrix} \begin{bmatrix} \bar{x}(t) - \bar{x}(t - \tau(t)) \\ \bar{x}(t - \tau(t)) - \bar{x}(t - \tau_M) \end{bmatrix} \\
= & \Theta^T(t) \Psi_5 \Theta(t).
\end{aligned} \tag{3.8}$$

Define the zero matrix:

$$0 = 2\theta_4^T(t) X(-\dot{\bar{x}}(t) + \bar{A}\bar{x}(t) + \bar{B}u(t) + \bar{F}v(t)). \tag{3.9}$$

Combining (3.6)–(3.9), the following inequality can be derived:

$$\dot{V}(t) \leq \theta^T(t) \left(\frac{(t_{k+1}h - t)}{h_k} F_1 + \frac{(t - t_k h)}{h_k} F_2 \right) \theta(t) - \bar{y}^T(t) \bar{y}(t) + \gamma^2 w^T(t) w(t), \tag{3.10}$$

where $F_1 = \Psi + h_k \Gamma_4 + \Gamma_2, F_2 = \Psi + h_k \Gamma_3 + \Gamma_1$.

By the Schur complement lemma and convex combination method, inequalities (3.2) and (3.3) can be derived from (3.10). Based on these inequalities, it can be further obtained that:

$$\dot{V}(t) \leq -\bar{y}^T(t)\bar{y}(t) + \gamma^2 w^T(t)w(t). \tag{3.11}$$

When $w(t) = 0$, $\dot{V}(t) \leq -\|\bar{y}(t)\|^2$, which indicates that system (2.15) satisfies the asymptotic stability condition. When $w(t) \in L_2[0, +\infty)$, since $\dot{V}(t)$ is continuous with respect to time t, integrating both sides of Eq (3.11) from 0 to $+\infty$ gives:

$$V(+\infty) - V(0) \leq \int_0^{+\infty} \left(-\bar{y}^T(t)\bar{y}(t) + \gamma^2 w^T(t)w(t)\right) dt. \tag{3.12}$$

Since $V(0) = 0$ and $V(+\infty) \geq 0$, we have $\|\bar{y}(t)\|_2 \leq \gamma\|w(t)\|_2$. Thus, it can be proved that when the NPS (9) satisfies the given conditions, it not only has asymptotic stability but also meets the H_∞ performance index requirement. □

Remark 3.1. *In the above Lyapunov functional, slack matrices and time-delay product terms are introduced to enhance the flexibility of stability analysis. Specifically, slack matrices effectively reduce the conservatism of stability criteria by providing additional degrees of freedom when handling matrix inequalities. Time-delay product terms, on the other hand, can better characterize the dynamic relationship between time-varying delays and system states, thereby describing the system's dynamic characteristics under delay effects more accurately. This combination not only simplifies the calculation process but also improves the precision of stability conditions, making the derived criteria more applicable to nonlinear power system scenarios with time-varying delays.*

Theorem 3.2. *For a given parameter τ_M, if there exist positive scalars α, β, σ, positive definite matrices $\bar{P}$, $\bar{Q}$, $\bar{R}_i(i = 1, 2, 3)$, $\bar{\Omega}$, $\bar{W}$, arbitrary matrices $\bar{M}_i(i = 1, 2)$, $\bar{N}_i(i = 1, 2)$ that satisfy $\begin{bmatrix} \bar{R} & \bar{S}^T \\ * & \bar{R} \end{bmatrix} > 0$, then the system (2.15) is asymptotically stable and has an H_∞ norm bound γ. When $\tau(t) = 0$ or τ_M, the following inequalities hold:*

$$\begin{bmatrix} \bar{\Psi} + h_k\Gamma_4 & \bar{\Upsilon}_1 & \bar{\Upsilon}_3 \\ * & -\bar{\Xi}_1 & 0 \\ * & * & -\Xi_3 \end{bmatrix} < 0, \tag{3.13}$$

$$\begin{bmatrix} \bar{\Psi} + h_k\Gamma_3 & \bar{\Upsilon}_2 & \bar{\Upsilon}_3 \\ * & -\bar{\Xi}_2 & 0 \\ * & * & -\Xi_3 \end{bmatrix} < 0, \tag{3.14}$$

$$\begin{bmatrix} -\rho \cdot I & (H\bar{C} - \bar{C}L)^T \\ * & -I \end{bmatrix} < 0, \tag{3.15}$$

where

$$
\begin{aligned}
&\bar{\Psi} = \sum_{i=0}^{6} \bar{\Psi}_i, \bar{\Psi}_1 = \alpha \cdot Sym\{e_2^T \bar{W}(e_1 - e_{11})\},\\
&\bar{\Psi}_2 = Sym\{\Pi_1^T \bar{P}\Pi_2\} + e_1^T \bar{Q} e_1 - e_3^T \bar{Q} e_3,\\
&\bar{\Psi}_3 = \tau_M^2 e_2^T \bar{R}_3 e_2 + \beta t_e Sym\{\Pi_3^T \bar{R}_3 \Pi_3 + t_e \Pi_4^T \bar{R}_3 \Pi_3\},\\
&\bar{\Psi}_4 = Sym\{\Pi_9^T \bar{M}_1 \Pi_5 + \Pi_9^T \bar{M}_2 \Pi_6\} + Sym\{\Pi_{10}^T \bar{\mathcal{N}}_1 \Pi_7 + \Pi_{10}^T \bar{\mathcal{N}}_2 \Pi_8\},\\
&\bar{\Psi}_5 = \Pi_{11}^T \begin{bmatrix} \bar{R} & \bar{S}^T, \\ * & \bar{R} \end{bmatrix} \Pi_{11}, \bar{\Psi}_6 = Sym\{\bar{I}_1 \bar{I}_2\} + e_1^T \bar{C}^T \bar{C} e_1 - e_{15}^T \gamma^2 I e_{15},\\
&\bar{I}_1 = \lambda_1 e_1^T + \lambda_2 e_2^T, \bar{I}_2 = \bar{A} L e_1 - L e_2 + \bar{B} L e_5 + \bar{F} L e_7, \quad \bar{\Xi}_1 = diag\{\bar{R}_2, 3\bar{R}_2\},\\
&\bar{\Upsilon}_1 = \begin{bmatrix} \sqrt{h_k}\Pi_{10}^T \bar{\mathcal{N}}_1 & \sqrt{h_k}\Pi_{10}^T \bar{\mathcal{N}}_2 \end{bmatrix}, \quad \bar{\Xi}_2 = diag\{\bar{R}_1, 3\bar{R}_1\},\\
&\bar{\Upsilon}_2 = \begin{bmatrix} \sqrt{h_k}\Pi_9^T \bar{M}_1 & \sqrt{h_k}\Pi_9^T \bar{M}_2 \end{bmatrix}, \bar{\Upsilon}_3 = \begin{bmatrix} \sigma I_1 H & \Pi_{12}^T \begin{bmatrix} \bar{C}D & \bar{C}D \end{bmatrix} \end{bmatrix}.
\end{aligned}
\tag{3.16}
$$

Define $L_m = T^{-1}$, $T_1 = \lambda_1 T$, $T_2 = \lambda_2 T$, $L_m = \text{diag}\overbrace{\{L, \ldots, L\}}^{m}$, and $\bar{P} = L_4^T P L_4$. Using the controller design method in [11], let $\bar{Q} = L_4^T Q L_4$, $\bar{R} = L^T R L (i = 1, 2, 3)$, $\bar{\Omega} = L^T \Omega L$, $\bar{W} = L^T W L$, $\bar{M}_i = L^T M_i L$ $(i = 1, 2)$, and $\bar{N}_i = L^T N_i L$ $(i = 1, 2)$. Additionally, define $K\bar{C}L \triangleq D\bar{C}$ and $\bar{C}L \triangleq H\bar{C}$. From this, we obtain $(H\bar{C} - \bar{C}L)^T (H\bar{C} - \bar{C}L) = 0$. Using the Schur complement lemma, this can be transformed into an optimization problem related to Eq (3.15). Multiply both sides of Eqs (3.2) and (3.3) by L_{10}^T on the left and L_{10} on the right, respectively, to derive Eqs (3.13) and (3.14). The gain matrix of the output feedback controller can be designed as $K = DH^{-1}$. This completes the proof of Theorem 3.2.

3.2. IGWO algorithm

For the standard GWO, its hierarchy is divided into four levels: α (head wolf), β (deputy head wolf), δ (auxiliary wolf), and ω (ordinary wolf). The core of the algorithm includes two stages: Encircling prey and hunting prey, with specific mathematical descriptions as follows: In the first stage, grey wolves gradually approach the prey through position updates, and their encircling behavior can be expressed as:

$$
\begin{cases}
D = |C \times X_P(t) - X(t)|, \\
X(t+1) = X_P(t) - A \times D,
\end{cases}
\tag{3.17}
$$

where A and C are behavior coefficient vectors, defined as: $A = 2a \cdot r_1 - a$, $C = 2r_2$. a is the convergence factor, which decreases linearly with the number of iterations, $a = 2 \times (1 - \frac{t}{t_{\max}})$, t is the current number of iterations, $t_{\max}$ is the maximum number of iterations, r_1 and r_2 are random vectors within $[0, 1]$, $X_P(t)$ is the prey position vector, and $X(t)$ is the current grey wolf position vector. In the second stage, during the hunting process, the ω wolf updates its position according to the positions of the α, β, and δ wolves:

$$
\begin{cases}
X_1 = X_\alpha(t) - A_1 D_1, \\
X_2 = X_\beta(t) - A_2 D_2, \\
X_3 = X_\delta(t) - A_3 D_3.
\end{cases}
\tag{3.18}
$$

The final position is determined by the weighted average of the positions of the three head wolves: $X(t+1) = \frac{X_1 + X_2 + X_3}{3}$. In the formula, $X_\alpha(t)$, $X_\beta(t)$, and $X_\delta(t)$ are the current positions of the α, β, and

δ wolves, respectively, and A_1, A_2, A_3 and D_1, D_2, D_3 are the corresponding head wolves' behavior coefficient vectors and distance vectors. The standard GWO realizes population iterative optimization through the above mechanism, but it has defects such as uneven initial population distribution and insufficient local search ability in the later stage due to the linear decrease of the convergence factor, which easily leads to falling into local optimum. Aiming at the above problems, the following improvement strategies are proposed: First, the tent chaotic mapping is used to generate the initial population to enhance the uniformity of the solution space distribution. The chaotic iteration formula is:

$$X(t+1) = \begin{cases} 2X(t), & 0 \le X(t) \le 0.5, \\ 2(1 - X(t)), & 0.5 < X(t) \le 1. \end{cases} \tag{3.19}$$

Combined with the lens learning mechanism, the initial solution is reversely optimized: $X'_{\text{in}} = X_{\min} + X_{\max} - \lambda_{\text{in}} X_{\text{in}}$, where X_{in} is the initial solution vector, X'_{in} is the improved solution, $X_{\min}$ and $X_{\max}$ are the minimum/maximum values of the solution vector, and λ_{in} is the chaotic sequence value.

Then, the linearly decreasing convergence factor is improved to an exponential nonlinear decreasing form:

$$a = a_{\text{in}} - (a_{\text{in}} - a_f)\frac{e^{\frac{t}{t_{\max}}} - 1}{e - 1}, \tag{3.20}$$

where a_{in} and a_f are the initial value and the final value of the convergence factor, respectively. This improvement makes the algorithm maintain strong global search ability in the early stage and enhance local fine optimization in the later stage.

Subsequently, the position update mechanism of the spider monkey optimization (SMO) algorithm is introduced, combined with the dynamic adjustment strategy of the inertia weight ω:

$$\begin{cases} X(t+1) = \omega \cdot \dfrac{X_1 + X_2 + X_3}{3} + a(X_{\text{gb}} - X) + a(X - X_1), \\ \omega = \omega_{\text{in}} - \dfrac{t}{t_{\max}}(\omega_{\text{in}} - \omega_f), \end{cases} \tag{3.21}$$

where ω_{in} and ω_f are the initial value and the final value of the inertia weight, respectively, and X_{gb} is the global optimal position. The linear decrease of the inertia weight balances the global exploration and local development capabilities of the algorithm.

Finally, a particle aggregation degree function is defined to determine the premature state of the population:

$$\rho = \frac{1}{d}\sum_{i=1}^{d}\left|\frac{f(X_i) - f_{\text{avg}}}{F}\right|^3, \quad F = \max\left\{1, \max\left|f(X_i) - f_{\text{avg}}\right|\right\}. \tag{3.22}$$

When the aggregation degree $\rho < K$ (mutation threshold $K = 0.5$), Cauchy perturbation is applied to the top 25% high-quality particles:

$$\begin{cases} \mathbf{X}_i = \mathbf{X}_i\left[1 + \left(\dfrac{t_{\max}}{t} - t\right) \times \text{Cauchy}(0,1)\right], \\ \text{Cauchy}(0,1) = \tan\left((r_{\text{and}} - 0.5) \times \pi\right), \end{cases} \tag{3.23}$$

where Cauchy$(0, 1)$ denotes the standard Cauchy perturbation random number, and r_{and} is a pseudo-random number uniformly distributed in $[0, 1]$. The flowchart of the algorithm is presented in Figure 2.

In this study, an IGWO algorithm is used to optimize the event-triggered parameter ε, aiming to ensure system stability and reduce bandwidth resource consumption. The following objective function is established: $\min J = \frac{N_{\text{trigger}}}{N_{\text{sample}}}$, where N_{trigger} represents the total number of trigger times, and N_{sample} is the total number of sampling times.

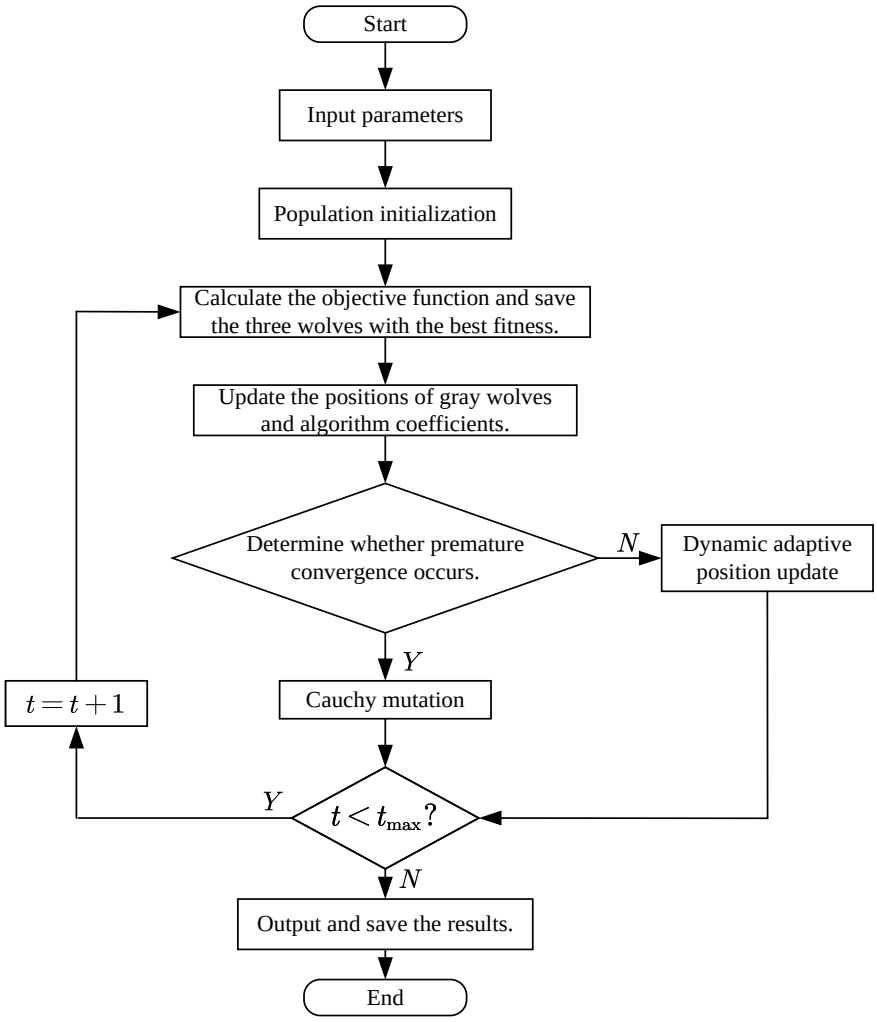

Figure 2. Flowchart of the IGWO algorithm.

4. Illustrative examples

In this section, the time-delay stability of a T-S fuzzy power system is first analyzed. Subsequently, a comparison between a conventional event-triggered scheme and an IGWO-optimized event-triggered scheme is conducted. The results demonstrate that the proposed method can significantly reduce bandwidth resource consumption while maintaining system stability, thereby validating its effectiveness. The parameters of the power system are listed in Table 2.

Table 2. Parameters of the power systems.

M	D	T_t	T_g	R	T_s	ρ_s
10.00	1.00	0.30	0.10	0.05	0.20	0.25
β	α_1, α_2	κ_e	T_e	ρ_e	K_s	K_f
21.00	0.500	1.00	0.10	1/21	0.30	0.20

4.1. Stability analysis of the T-S fuzzy power system

For the T-S fuzzy power system, first, the convex combination technique is used to reconstruct the nonlinear term $\xi(\Delta p_g(t))$, so as to establish a T-S fuzzy system model with an analytical form. Considering the number of fuzzy rules m, when m is small (e.g., $m = 1$), the computational load is small but the accuracy is low. When m is large (e.g., $m = 3$), the accuracy is high but the computation is complex. Since $\xi(\Delta p_g(t))$ only needs 2 rules to cover all its nonlinear behaviors, $m = 2$ is chosen to ensure the optimal balance between model accuracy and computational complexity. It is assumed that $\Delta p_g(t) \in [\Omega_L, \Omega_U]$, and the following relationships are considered:

$$\begin{cases} \xi(\Delta p_g(t)) = L_1(\Delta p_g(t))\Delta p_g(t) + \eta L_2(\Delta p_g(t))\Delta p_g(t), \\ L_1(\Delta p_g(t)) + L_2(\Delta p_g(t)) = 1, \end{cases} \tag{4.1}$$

where $\eta = \min\left(\left|\frac{\xi_{\min}}{\Omega_L}\right|, \left|\frac{\xi_{\max}}{\Omega_U}\right|\right)$. Solving Eq (4.1) yields:

$$\begin{cases} L_1(\Delta p_g(t)) = \dfrac{\xi(\Delta p_g(t)) - \eta\Delta p_g(t)}{(1-\eta)\Delta p_g(t)}, \\ L_2(\Delta p_g(t)) = \dfrac{\Delta p_g(t) - \xi(\Delta p_g(t))}{(1-\eta)\Delta p_g(t)}. \end{cases} \tag{4.2}$$

The dynamic characteristics of the power system can then be described by the following fuzzy rules:

Rule 1: If $\Delta p_g(t)$ is $L_1(\Delta p_g(t))$, then $\dot{\bar{x}}(t) = A_1\bar{x}(t) + B_1u(t_kh) + F_1w(t)$.

Rule 2: If $\Delta p_g(t)$ is $L_2(\Delta p_g(t))$, then $\dot{\bar{x}}(t) = A_2\bar{x}(t) + B_2u(t_kh) + F_2w(t)$, where $B_1 = B_2 = B$ and $F_1 = F_2 = F$. The system matrices are given by:

$$A_1 = \begin{bmatrix} -\frac{D}{M} & \frac{1}{M} & 0 & \frac{1}{M} & 0 \\ 0 & -\frac{1}{T_t} & \frac{1}{T_t} & 0 & 0 \\ -\frac{1}{T_gR} & 0 & -\frac{1}{T_g} & 0 & 0 \\ -\frac{\rho_e\kappa_e}{T_e} & 0 & 0 & -\frac{1}{T_e} & 0 \\ \beta & 0 & 0 & 0 & 0 \end{bmatrix}, \quad A_2 = \begin{bmatrix} -\frac{D}{M} & \frac{1}{M} & 0 & \frac{1}{M} & 0 \\ 0 & -\frac{1}{T_t} & \frac{\eta}{T_t} & 0 & 0 \\ -\frac{1}{T_gR} & 0 & -\frac{\eta}{T_g} & 0 & 0 \\ -\frac{\rho_e\kappa_e}{T_e} & 0 & 0 & -\frac{1}{T_e} & 0 \\ \beta & 0 & 0 & 0 & 0 \end{bmatrix}. \tag{4.3}$$

The defuzzified system dynamics are expressed as:

$$\dot{\bar{x}}(t) = \sum_{i=1}^{2}\sum_{j=1}^{2} \nu_i\nu_j \left(A_i\bar{x}(t) - B_iK_jC_i\bar{x}(t-\tau(t)) - B_iK_jC_ie(t) + F_iw(t)\right). \tag{4.4}$$

The allowable upper bounds of time-varying delays obtained by solving the stability criteria of Theorem 3.1 using the LMIs toolbox are shown in Table 3. It can be seen that the upper bound of

time-varying delays in this paper is larger than that in paper [38], verifying that the stability criteria in this paper have lower conservatism. In addition, to compare the complexity of the method in this paper with other methods, Table 4 lists the complexity indicators of several key criteria, where N_D is the total number of decision variables and N_R is the total number of rows of all linear matrix inequalities (LMIs). By substituting the values of N_D and N_R in Table 4 into the formula $O(n) = N_D^2 N_R^{2.5} + N_R^{3.5}$ [39] solved by the commonly used SeDuMi solver, it can be clearly seen that the $O(n)$ of the method in this paper is significantly lower than that in the recent study [40]. This indicates that the method in this paper has higher computational efficiency while ensuring stability.

Table 3. Time-varying delay upper bound.

Methods	$[K_P, K_I]$		
	$[0.10, 0.05]$	$[0.10, 0.10]$	$[0.10, 0.15]$
Method [41]	9.330	11.723	10.563
Theorem 3.1	9.420	11.812	10.637
Improvement	0.964%	0.759%	0.701%

Table 4. Numerical complexity of system (4.4).

	N_D	N_R	$O(n)(n = 2)$
Th. 1 [42]	$49n^2 + 5n$	$70n$	9.86×10^9
Th. 1 [40]	$177.5n^2 + 6.5n + 2nm$	$301n$	4.69×10^{12}
Th. 1	$167n^2 + 28n$	$258n$	3.174×10^{12}

4.2. Case study of the general ETM

Case 1: For the triggering mechanism in general situations, the event-triggered parameter is a fixed constant. Let the event-triggered parameter $\varepsilon = 0.01$, the load disturbance $\varphi(t) = 0.2\sin(t)$, the time-varying delay $\tau(t) = 0.8\sin^2(t) + 0.8$, and the initial state of the NPS be set as $\overline{x}(0) = \text{col}\{0.036, 0.021, -0.045, -0.025, 0.034, -0.013\}$. By solving the LMIs in Theorem 3.2, the PI control gains can be obtained as $[K_{P1}, K_{I1}] = [0.0326, -0.2461]$ and $[K_{P2}, K_{I2}] = [0.0270, -0.2458]$. The state response curve of the NPS is shown in Figure 3. It can be seen from the figure that the state curve eventually converges, fully verifying the effectiveness of the designed PI controller. The event-triggered time intervals are shown in Figure 4. Through calculation, the average event-triggered interval is 0.28.

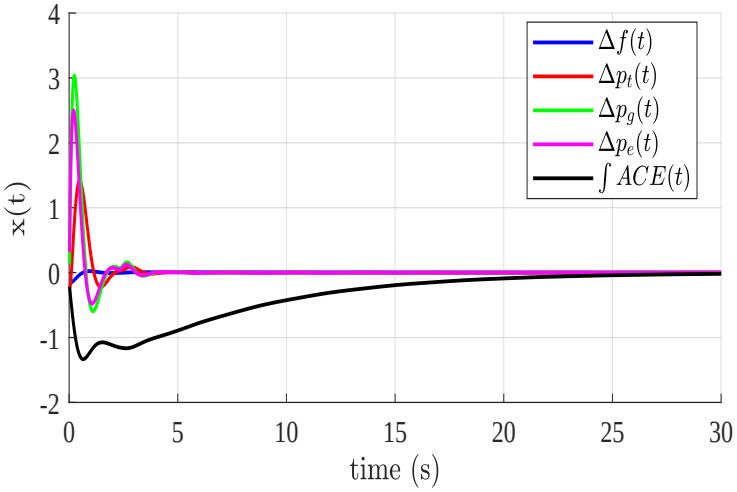

Figure 3. State responses of the NPS.

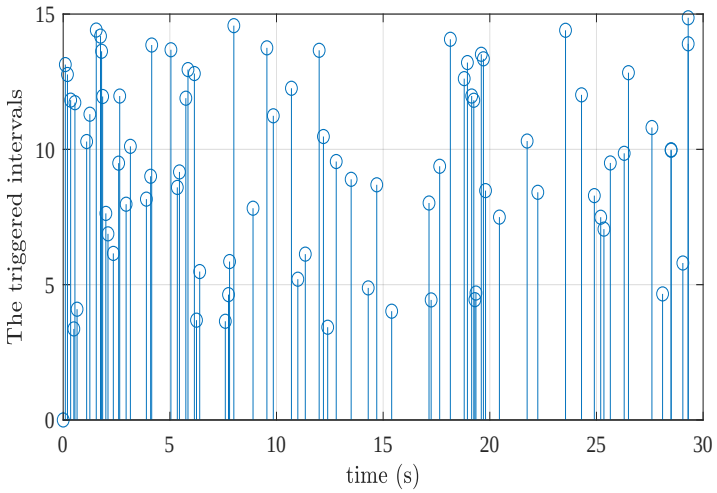

Figure 4. Event-triggered instants.

4.3. Case study of the optimized ETM

Case 2: When using the GWO algorithm to optimize the ETM, we take the event-triggered threshold parameters μ and v as optimization variables, and set the grey wolf population size to 40, the maximum number of iterations to 150, and the weight coefficients $\omega_1 = 0.6$, $\omega_2 = 0.3$, $\omega_3 = 0.1$. By solving the linear matrix inequalities (LMIs), the PI control gains are derived as $[K_{P1}, K_{I1}] = [0.0247, -0.3542]$ and $[K_{P2}, K_{I2}] = [0.0364, -0.2643]$.

The state response trajectory and event-triggered intervals are shown in Figures 5 and 6, respectively.

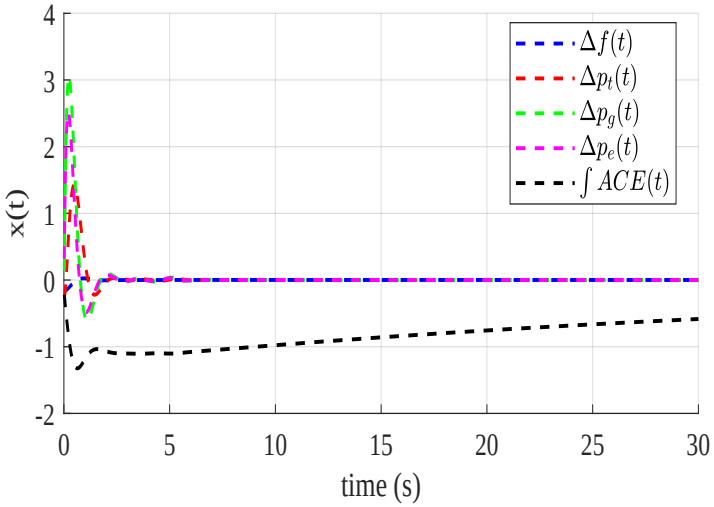

Figure 5. State responses of the NPS optimized by GWO.

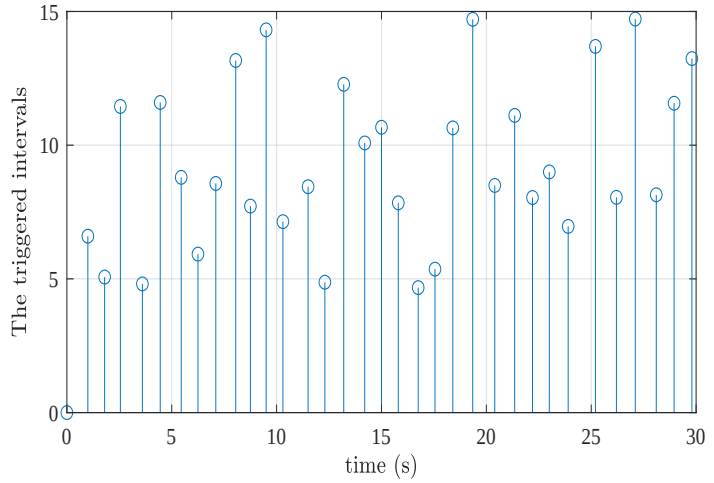

Figure 6. Event-triggered instants optimized by GWO.

Case 3: When using the IGWO algorithm to optimize the ETM, we set the population size to 30, the maximum number of iterations to 100, the weight coefficients $\omega_1 = 0.7$, $\omega_2 = 0.2$, $\omega_3 = 0.1$, and the initial and final values of the exponential convergence factor as $a_{\text{in}} = 2$ and $a_{\text{f}} = 0$, respectively. Finally, by solving the linear matrix inequalities (LMIs), the PI control gains are obtained as $[K_{P1}, K_{I1}] = [0.0371, -0.2541]$ and $[K_{P2}, K_{I2}] = [0.0387, -0.2130]$.

The state response trajectory and event-triggered intervals are shown in Figures 7 and 8, respectively.

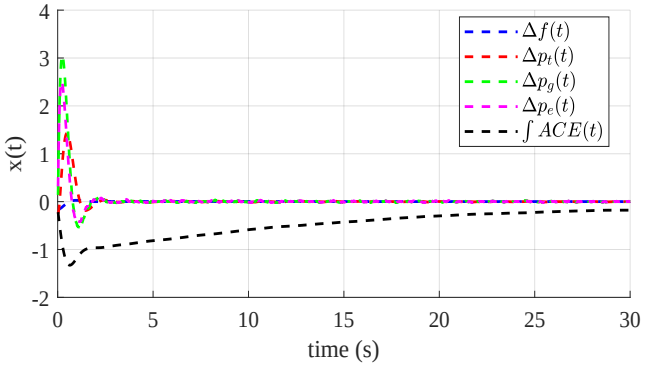

Figure 7. State responses of the NPS optimized by IGWO.

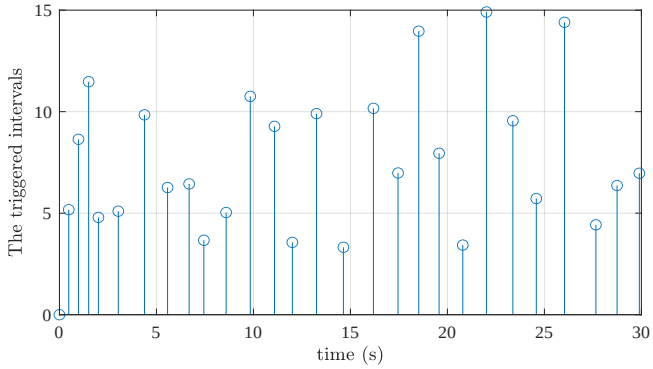

Figure 8. Event-triggered instants optimized by IGWO.

Comparing the experimental results of Case 1, Case 2, and Case 3 shows that the average event-triggered intervals are 0.28, 1.273, and 1.534, respectively. This clearly indicates that the trigger mechanism optimized by GWO significantly increases the average trigger interval compared with the unoptimized case, while the further improved GWO-based triggering mechanism has more advantages in increasing the triggering interval than the conventional GWO method.In terms of data transmission efficiency, the IGWO trigger mechanism proposed in this paper only needs to send 47 data packets, which is much less than the 199 packets required by the ordinary trigger mechanism, effectively reducing the data transmission volume by approximately 76.4%. By simply calculating the average trigger interval of the proposed method and comparing it with the results in other literatures, as shown in Table 5, it is found that the average trigger interval is increased by 38.2% compared with [38].

Table 5. The average intervals using different triggering mechanisms.

Triggering mechanisms	Average intervals
Time-triggering mechanism [43]	0.180
Memory-based ETM [38]	1.110
ETM optimized by IGWO	1.534

5. Conclusions

This paper studies the load frequency control problem of power systems integrated with an ETM and an IGWO algorithm. First, an NPS model including an ESS and RESs is constructed, and the T-S fuzzy theory is adopted to handle the nonlinear terms in the model, laying a foundation for subsequent research. Second, an ETM is introduced, and the IGWO algorithm is used to find the optimal event-triggered parameters, which effectively reduces unnecessary information transmission and improves the utilization efficiency of communication resources. In addition, based on the Lyapunov functional stability theory, a stability criterion compatible with time-varying delays and nonlinearity is derived, and a corresponding controller is designed to ensure the stability and control effectiveness of the system. Finally, comparative simulations verify the superiority and effectiveness of the proposed method, demonstrating that the optimization method can ensure the stability and control performance of the system while reducing the bandwidth resource consumption. In the future, the application of this method in other complex power system scenarios can be further explored to address more challenges.

Author contributions

Yan Chen: Conceptualization, methodology, investigation, code writing, writing-original draft, validation; Xingyue Liu: Writing-review and editing, supervision, methodology, formal analysis, conceptualization; Kaibo Shi: Writing-review and editing, supervision, validation; Fengying Zeng: Conceptualization, methodology, software; Fanglu Yang: Validation, supervision, methodology. All authors have read and approved the final version of the manuscript for publication.

Use of Generative-AI tools declaration

The authors declare that they have not used Artificial Intelligence (AI) tools in the creation of this article.

Acknowledgments

This work was supported by the Sichuan Science and Technology Program under Grant No. 21YYJC0469, National Natural Science Foundation of China under Grant Nos. 61703060 and 12061088 , Guangdong Basic and Applied Basic Research Foundation (2021A1515011692), Engineering Research Center of Power Quality of Ministry of Education, Anhui University (No. KFKT202102), and Open Research Fund Program of Data Recovery Key Laboratory of Sichuan Province (Grant No. DRN2103).

Conflict of interest

The authors declare there is no conflict of interest in this paper.

References

1. A. Oshnoei, M. Kheradmandi, S. M. Muyeen, Robust control scheme for distributed battery energy storage systems in load frequency control, *IEEE Trans. Power Syst.*, **35** (2020), 4781–4791. https://doi.org/10.1109/TPWRS.2020.2997950
2. S. Zhang, Y. Mishra, M. Shahidehpour, Fuzzy-logic based frequency controller for wind farms augmented with energy storage systems, *IEEE Trans. Power Syst.*, **31** (2016), 1595–1603. https://doi.org/10.1109/TPWRS.2015.2432113
3. C. T. Pan, C. M. Liaw, An adaptive controller for power system load-frequency control, *IEEE Trans. Power Syst.*, **4** (1989), 122–128. https://doi.org/10.1109/59.32469
4. Z. Cheng, S. Hu, D. Yue, C. Dou, S. Shen, Resilient distributed coordination control of multiarea power systems under hybrid attacks, *IEEE Trans. Syst. Man Cybernet. Syst.*, **52** (2022), 7–18. https://doi.org/10.1109/TSMC.2021.3049373
5. X. C. Shangguan, C. K. Zhang, Y. He, L. Jin, L. Jiang, J. W. Spencer, et al., Robust load frequency control for power system considering transmission delay and sampling period, *IEEE Trans. Ind. Inform.*, **17** (2021), 5292–5303. https://doi.org/10.1109/TII.2020.3026336
6. K. Liao, Y. Xu, A robust load frequency control scheme for power systems based on second-order sliding mode and extended disturbance observer, *IEEE Trans. Ind. Inform.*, **14** (2017), 3076–3086. https://doi.org/10.1109/TII.2017.2771487
7. X. C. Shangguan, Y. He, C. K. Zhang, L. Jiang, M. Wu, Adjustable event-triggered load frequency control of power systems using control-performance-standard-based fuzzy logic, *IEEE Trans. Fuzzy Syst.*, **30** (2022), 3297–3311. https://doi.org/10.1109/TFUZZ.2021.3112232
8. X. Chen, S. Hu, Y. Li, D. Yue, C. Dou, L. Ding, Co-estimation of state and FDI attacks and attack compensation control for multi-area load frequency control systems under FDI and DoS attacks, *IEEE Trans. Smart Grid*, **13** (2022), 2357–2368. https://doi.org/10.1109/TSG.2022.3147693
9. W. Huimin, Z. S. Li, Multi-area load frequency control in power system integrated with wind farms using fuzzy generalized predictive control method, *IEEE Trans. Reliability*, **72** (2022), 737–747. https://doi.org/10.1109/TR.2022.3177045
10. C. Peng, J. Li, M. Fei, Resilient event-triggering H_∞ load frequency control for multi-area power systems with energy-limited DoS attacks, *IEEE Trans. Power Syst.*, **32** (2017), 4110–4118. https://doi.org/10.1109/TPWRS.2016.2634122
11. Q. Zhong, J. Yang, K. Shi, S. Zhong, Z. Li, M. A. Sotelo, Event-triggered H_∞ load frequency control for multi-area nonlinear power systems based on non-fragile proportional integral control strategy, *IEEE Trans. Intell. Transp. Syst.*, **23** (2022), 12191–12201. https://doi.org/10.1109/TITS.2021.3110759
12. X. Li, D. Ye, Event-based distributed fuzzy load frequency control for multiarea nonlinear power systems with switching topology, *IEEE Trans. Fuzzy Syst.*, **30** (2022), 4262–4272. https://doi.org/10.1109/TFUZZ.2022.3146981
13. Z. Wang, J. Wang, M. La Scala, A novel distributed-decentralized fixed-time optimal frequency and excitation control framework in a nonlinear network-preserving power system, *IEEE Trans. Power Syst.*, **36** (2021), 1285–1297. https://doi.org/10.1109/TPWRS.2020.3011156

14. Z. Hu, S. Liu, W. Luo, L. Wu, Resilient distributed fuzzy load frequency regulation for power systems under cross-layer random denial-of-service attacks, *IEEE Trans. Cybernet.*, **52** (2022), 2396–2406. https://doi.org/10.1109/TCYB.2020.3005283

15. K. Tanaka, M. Sugeno, Stability analysis and design of fuzzy control systems, *Fuzzy Sets Syst.*, **45** (1992), 135–156. https://doi.org/10.1016/0165-0114(92)90113-I

16. S. Sui, C. L. P. Chen, S. Tong, Command filter-based predefined time adaptive control for nonlinear systems, *IEEE Trans. Automat. Control*, **69** (2024), 7863–7870. https://doi.org/10.1109/TAC.2024.3399998

17. S. Tong, S. Sui, Y. Li, Fuzzy adaptive output feedback control of MIMO nonlinear systems with partial tracking errors constrained, *IEEE Trans. Fuzzy Syst.*, **23** (2015), 729–742. https://doi.org/10.1109/TFUZZ.2014.2327987

18. Z. J. Wang, F. Liu, J. Z. F. Pang, S. H. Low, S. W. Mei, Distributed optimal frequency control considering a nonlinear network-preserving model, *IEEE Trans. Power Syst.*, **34** (2019), 76–86. https://doi.org/10.1109/TPWRS.2018.2861941

19. Y. Dong, Y. Song, G. Wei, Efficient model-predictive control for nonlinear systems in interval type-2 T-S fuzzy form under round-robin protocol, *IEEE Trans. Fuzzy Syst.*, **30** (2022), 63–74. https://doi.org/10.1109/TFUZZ.2020.3031394

20. M. C. Valentino, F. A. Faria, V. A. Oliveira, L. F. C. Alberto, Ultimate boundedness sufficient conditions for nonlinear systems using T-S fuzzy modelling, *Fuzzy Sets Syst.*, **361** (2019), 88–100. https://doi.org/10.1016/j.fss.2018.03.010

21. Y. Li, K. Yu, Adaptive fuzzy decentralized sampled-data control for large-scale nonlinear systems, *IEEE Trans. Fuzzy Syst.*, **30** (2022), 1809–1822. https://doi.org/10.1109/TFUZZ.2021.3069321

22. A. Seuret, A novel stability analysis of linear systems under asynchronous samplings, *Automatica*, **48** (2012), 177–182. https://doi.org/10.1016/j.automatica.2011.09.033

23. L. Dong, Y. Tang, H. He, C. Sun, An event-triggered approach for load frequency control with supplementary ADP, *IEEE Trans. Power Syst.*, **32** (2017), 581–589. https://doi.org/10.1109/TPWRS.2016.2537984

24. X. C. Shangguan, S. Shi, Y. He, C. K. Zhang, Optimal digital load frequency control of smart grid considering sampling and time delay based on warm-up gray wolf algorithm, *IEEE Trans. Ind. Inform.*, **21** (2025), 1773–1782. https://doi.org/10.1109/TII.2024.3485821

25. X. Sun, C. Hu, G. Lei, Y. Guo, J. Zhu, State feedback control for a PM hub motor based on grey wolf optimization algorithm, *IEEE Trans. Power Electron.*, **35** (2020), 1136–1146. https://doi.org/10.1109/TPEL.2019.2923726

26. Y. He, Q. G. Wang, C. Lin, M. Wu, Augmented Lyapunov functional and delay-dependent stability criteria for neutral systems, *Int. J. Robust Nonlinear Control*, **15** (2005), 923–933. https://doi.org/10.1002/rnc.1039

27. J. Chen, J. H. Park, S. Xu, B. Zhang, A survey of inequality techniques for stability analysis of time-delay systems, *Int. J. Robust Nonlinear Control*, **32** (2022), 6412–6440. https://doi.org/10.1002/rnc.6151

28. J. H. Kim, Further improvement of Jensen inequality and application to stability of time-delayed systems, *Automatica*, **64** (2016), 121–125. https://doi.org/10.1016/j.automatica.2015.08.025

29. A. Seuret, F. Gouaisbaut, Wirtinger-based integral inequality: Application to time-delay systems, *Automatica*, **49** (2013), 2860–2866. https://doi.org/10.1016/j.automatica.2013.05.030

30. Z. Cheng, S. Hu, D. Yue, C. Dou, S. Shen, Resilient distributed coordination control of multiarea power systems under hybrid attacks, *IEEE Trans. Syst. Man Cybern. Syst.*, **52** (2021), 7–18. https://doi.org/10.1109/TSMC.2021.3049373

31. L. Jin, Y. He, C. Ke. Zhang, X. C. Shangguan, L. Jiang, M. Wu, Robust delay-dependent load frequency control of wind power system based on a novel reconstructed model, *IEEE Trans. Cybernet.*, **52** (2022), 7825–7836. https://doi.org/10.1109/TCYB.2021.3051160

32. H. B. Zeng, S. J. Zhou, X. M. Zhang, W. Wang, Delay-dependent stability analysis of load frequency control systems with electric vehicles, *IEEE Trans. Cybernet.*, **52** (2022), 13645–13653. https://doi.org/10.1109/TCYB.2022.3140463

33. C. Peng, J. Zhang, H. Yan, Adaptive event-triggering H_∞ load frequency control for network-based power systems, *IEEE Trans. Ind. Electron.*, **65** (2018), 1685–1694. https://doi.org/10.1109/TIE.2017.2726965

34. J. Yang, Q. Zhong, K. Shi, Y. Yu, S. Zhong, Stability and stabilization for T-S fuzzy load frequency control power system with energy storage system, *IEEE Trans. Fuzzy Syst.*, **32** (2023), 893–905. https://doi.org/10.1109/TFUZZ.2023.3311925

35. P. G. Park, J. W. Ko, C. Jeong, Reciprocally convex approach to stability of systems with time-varying delays, *Automatica*, **47** (2011), 235–238. https://doi.org/10.1016/j.automatica.2010.10.014

36. H. B. Zeng, Y. He, M. Wu, J. She, Free-matrix-based integral inequality for stability analysis of systems with time-varying delay, *IEEE Trans. Automat. Control*, **60** (2015), 2768–2772. https://doi.org/10.1109/TAC.2015.2404271

37. T. H. Lee, J. H. Park, A novel Lyapunov functional for stability of time-varying delay systems via matrix-refined-function, *Automatica*, **80** (2017), 239–242. https://doi.org/10.1016/j.automatica.2017.02.004

38. E. Tian, C. Peng, Memory-based event-triggering H_∞ load frequency control for power systems under deception attacks, *IEEE Trans. Cybernet.*, **50** (2020), 4610–4618. https://doi.org/10.1109/TCYB.2020.2972384

39. D. Xiong, C. K. Zhang, L. Jin, Y. L. Fan, Y. He, Stability and stabilization of T-S fuzzy systems with sampled-data controller: A fuzzy-related matrix injection method, *IEEE Trans. Fuzzy Syst.*, **33** (2025), 2549–2560. https://doi.org/10.1109/TFUZZ.2025.3568518

40. G. Velmurugan, Y. H. Joo, Sampled-data control design for T-S fuzzy system via quadratic function negative-determination approach, *IEEE Trans. Fuzzy Syst.*, **32** (2024), 979–988. https://doi.org/10.1109/TFUZZ.2023.3316351

41. L. Shanmugam, Y. H. Joo, Stability and stabilization for T-S fuzzy large-scale interconnected power system with wind farm via sampled-data control, *IEEE Trans. Syst. Man Cybern. Syst.*, **51** (2021), 2134–2144. https://doi.org/10.1109/TSMC.2020.2965577

42. F. Yang, S. Guan, D. Wang, Quadratically convex combination approach to stability of T-S fuzzy systems with time-varying delay, *J. Franklin Inst.*, **351** (2014), 3752–3765. https://doi.org/10.1016/j.jfranklin.2013.01.025

43. H. Zhang, J. Yang, C. Su, T-S fuzzy-model-based robust H_∞ design for networked control systems with uncertainties, *IEEE Trans. Ind. Informat.*, **3** (2007), 289–301. https://doi.org/10.1109/TII.2007.911895

AIMS Press

© 2025 the Author(s), licensee AIMS Press. This is an open access article distributed under the terms of the Creative Commons Attribution License (https://creativecommons.org/licenses/by/4.0)